Bond ordering and phase transitions in Na₂IrO₃ under high pressure

Kaige Hu,[1,2] Zhimou Zhou,[1] Yi-Wen Wei,[1] Chao-Kai Li,[1] and Ji Feng[1,3,4,*]

[1]*International Center for Quantum Materials, School of Physics, Peking University, Beijing 100871, China*
[2]*School of Physics and Optoelectronic Engineering, Guangdong University of Technology, Guangzhou 510006, China*
[3]*Collaborative Innovation Center of Quantum Matter, Beijing 100871, China*
[4]*CAS Center for Excellence in Topological Quantum Computation, University of Chinese Academy of Sciences, Beijing 100190, China*

The Kitaev model of spin-1/2 on a honeycomb lattice supports degenerate topological ground states and may be useful in topological quantum computation. Na₂IrO₃ with a honeycomb lattice of Ir ions has been extensively studied as a candidate for the realization of this model, due to the effective $J_{\mathrm{eff}} = 1/2$ low-energy excitations produced by the spin-orbit and crystal-field effect. As the eventual realization of the Kitaev model has remained evasive, it is highly desirable and challenging to tune the candidate materials toward such an end. It is well known that external pressure often leads to dramatic changes in the geometric and electronic structure of materials. In this Rapid Communication, the high-pressure phase diagram of Na₂IrO₃ is examined by first-principles calculations. It is found that Na₂IrO₃ undergoes a sequence of structural and magnetic phase transitions, from a magnetically ordered phase with space group $C2/m$ to two bond-ordered nonmagnetic phases. The low-energy excitations in these high-pressure phases can be well described by the $J_{\mathrm{eff}} = 1/2$ states.

In recent years the Kitaev model [1], an exactly solvable two-dimensional spin-1/2 model on a honeycomb lattice with distortional nearest-neighbor interactions, has attracted considerable attention. The Kitaev ground state is a quantum spin liquid with possible non-Abelian anyonic excitations, whose realization will be an important step towards topological quantum computation [1]. To date, $5d$ iridates $A_2\mathrm{IrO}_3(A = \mathrm{Na},$ Li) [2–18] have been extensively studied for the realization of the Kitaev model. However, the ground states of these materials are not the desired spin liquid, but all magnetically ordered [4–13]. It turns out that the existence of Heisenberg interactions and also off-diagonal interactions plays an important role in determining the magnetic configuration of the ground state [13–15], and the magnetic configuration is sensitive to structure deviations [13].

Although the Kitaev model has not been realized in iridates, many studies indicate that the Kitaev terms are the dominant interactions and the systems are near the spin-liquid region in the parameter phase diagrams [11–13,15,16]. Therefore, it may be possible to find new Kitaev materials whose parameters fortunately locate in the zone of the Kitaev spin-liquid phase. Recent studies on α-RuCl₃, OsCl₃, Cu₂IrO₃, and H₃LiIr₂O₆ have made progress in this direction [19–22]. In addition, the electronic states of these candidate materials can be changed dramatically by the application of external fields or pressure. Pressure can even introduce dramatic geometric changes to these materials. Therefore, whether these candidate materials can be tuned to the Kitaev ground state will be an essential question. To date, magnetic-field-induced quantum spin-liquid phases have been reported in α-RuCl₃, however, the experimental data cannot be reconciled with

the behavior of the Kitaev spin liquid [23,24]. Pressure-induced melting of the magnetic order is observed in α-RuCl₃ [25–27]. Structural and magnetic transitions under pressure are observed in iridate α-Li₂IrO₃ [17]. As the first condensed matter candidate for the Kitaev model, however, Na₂IrO₃ shows no sign of a structural phase transition in previous experiments under high pressures up to 24 GPa [18].

In this Rapid Communication, we study the phase transitions in Na₂IrO₃ under high pressure by first-principles calculations. In Na₂IrO₃, each Ir⁴⁺ ion is surrounded by an oxygen octahedron and the crystal field splits d orbitals into e_g and t_{2g} orbitals, and, further, strong spin-orbit coupling (SOC) leads to an effective pseudospin-1/2. The interest in a possible exotic quantum phase in Na₂IrO₃ is accompanied by many revisions of its structure, magnetic configuration, and microscopic model [3–9,13–16]. It may reflect the complexity of $5d$ transition-metal oxides due to the interplay of SOC, electron correlation, and crystal-field splitting effects, all of which can be modified in nontrivial ways by the application of external pressure. Indeed, we find remarkable nonmagnetic (NM) ground states of Na₂IrO₃ under high pressure, in which $J_{\mathrm{eff}} = 1/2$ states are still dominant in the low-energy region. The magnetic phase transition is seen to be induced by bond ordering, where local structure dimerization is formed with long-range order, with a concomitant electronic phase transition from a Mott insulator to band insulators. The bond-ordered nonmagnetic phase may bear a remarkable resemblance to the gapped A phase of the Kitaev ground state [1].

We perform noncollinear relativistic density functional theory (DFT) calculations with full self-consistent fields, as implemented in the Vienna *ab initio* simulation package (VASP) [28–30]. The projector augmented-wave potentials with a plane-wave cutoff of 500 eV are employed. We set
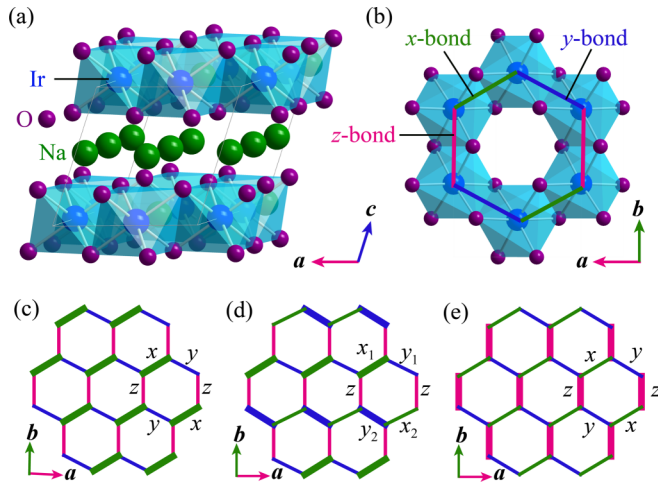
*jfeng11@pku.edu.cn

FIG. 1. (a) Crystal structure of $C2/m$, viewed from slightly off the $\boldsymbol{b}$ direction. (b) Nearly ideal Ir honeycomb lattice of $C2/m$, viewed from the direction perpendicular to the ab plane. Green, blue, and magenta bonds are x, y, and z bonds, respectively. The bond length relation is $l_x = l_y \lesssim l_z$. The Ir honeycomb lattice of (c) $P\bar{1}$ with shorter x bonds, $l_x < l_y \approx l_z$, (d) $P2_1/m$ with shorter x_1 and y_2 bonds, $l_{x_1} = l_{y_2} < l_{x_2} = l_{y_1} \approx l_z$, and (e) $C2/m$-zz with shorter z bonds, $l_z < l_x = l_y$. Note that all short Ir-Ir bonds in (c)–(e) are highlighted by thicker lines.

$U = 1.7$ eV [13] and $J = 0.6$ eV [31], corresponding to a choice of effectively $U_{\mathrm{eff}} = U - J = 1.1$ eV [32] for all the structures under consideration, unless otherwise specified. The energy convergence criteria is 10^{-5} eV and the interatomic force convergence for structure optimizations is 0.01 eV/Å. Hydrostatic pressures are adopted in our high-pressure study, i.e., pressures are isotropic in all directions. Phonon dispersions are calculated by the finite displacement method [33,34], where a $2 \times 2 \times 2$ supercell is adopted.

Under ambient pressure, Na$_2$IrO$_3$ is a layered compound of space group $C2/m$ (No. 12) [6,7], whose atom layers are stacked repeating the sequence O-Ir$_{2/3}$Na$_{1/3}$-O-Na, as shown in Fig. 1(a). Each ion in the structure has six oppositely charged ions as the first neighbors forming octahedral cages, akin to a distorted rocksalt structure. Figure 1(a) highlights the IrO$_6$ octahedrons particularly. The atom layers are in the ab plane. In each Ir$_{2/3}$Na$_{1/3}$ layer, Ir^{4+} ions form a honeycomb lattice, with Na$^+$ ions at the center of the hexagons. There are three types of nearest-neighbor Ir-Ir links named as x, y, and z bonds [Fig. 1(b)], respectively. This nomenclature is derived from the fact that those bonds are perpendicular to the cubic $\mathbf{x}$, $\mathbf{y}$, and $\mathbf{z}$ axes of the parent rocksalt structure, respectively. The Ir honeycomb lattice is nearly ideal, with z bonds slightly longer than x and y bonds, i.e., $l_x = l_y \lesssim l_z$, where l_x, l_y, and l_z are bond lengths of x, y, and z bonds, respectively. The Ir honeycomb lattice becomes zigzag antiferromagnetic (AFM) below $T_N = 15$ K [4–7], and neighboring Ir layers are also antiferromagnetically coupled [5]. We call this ground structure $C2/m$-zigzag. Within the zigzag AFM phase, the direction of magnetization is $\boldsymbol{g} \approx \boldsymbol{a} + \boldsymbol{c}$, located in the cubic xy plane of the IrO$_6$ octahedron and pointing to the center of the O-O edge [9,13]. Despite the AFM stacking Ir honeycomb layers, only one Ir layer needs to be considered in the Kitaev-

Heisenberg (KH) model since the interactions between Ir honeycomb layers are negligible [13].

Under high pressure, two new crystal structures are found, whose space groups are $P\bar{1}$ (No. 2) and $P2_1/m$ (No. 11), respectively. Their structural stabilities are verified by phonon dispersion calculations (see the Supplemental Material [35]). The key structural feature of these high-pressure phases is the emergence of bond ordering. For $P\bar{1}$ shown in Fig. 1(c), y bonds and z bonds are elongated to the same extent whereas the x bonds are shrunk distinctly, i.e., $l_x < l_y \approx l_z$. $P2_1/m$ shown in Fig. 1(d) displays yet another bond ordering: x and y bonds are further separated into two types, i.e., x_1, x_2 and y_1, y_2, respectively, where z bonds, x_2 bonds, and y_1 bonds are elongated to some extent while remaining almost equal to each other, but x_1 bonds and y_2 bonds are shrunk, i.e., $l_{x_1} = l_{y_2} < l_{x_2} = l_{y_1} \approx l_z$. It is worth mentioning that a third type of bond ordering shown in Fig. 1(e) is also possible as a metastable structure at high pressures, where z bonds are shrunk, i.e., $l_z < l_x = l_y$. The space group remains $C2/m$, therefore we call this structure $C2/m$-zz. As shown in Figs. 1(c) and 1(e), $C2/m$-zz takes on a similar bond ordering just as $P\bar{1}$. We find $P\bar{1}$, $P2_1/m$, and $C2/m$-zz are all NM band insulators.

According to our calculations, there is no structural phase transition below 24 GPa, which is consistent with a previous experiment [18]. However, at about 36 GPa, a structural phase transition is found computationally, and the new phase (space group $P\bar{1}$) is seen to be enthalpically favored up to 42 GPa. Since the $P\bar{1}$ structure is NM, there is simultaneously a magnetic phase transition at about 36 GPa. At the same time, the system transforms from a Mott insulator to a band insulator. At about 42 GPa, the computed enthalpies indicate the Na$_2$IrO$_3$ enters a new structural phase with space group $P2_1/m$, which remains NM. Figures 2(a) and 2(b) show the enthalpy for $C2/m$, $P\bar{1}$, and $P2_1/m$ structures relative to the $C2/m$-zigzag structure and the $P2_1/m$ structure, respectively. A new energy reference is needed for higher pressures since the $C2/m$-zigzag structure cannot exist under pressures higher than 48 GPa. For completeness, bilayer cases of (1) one layer with short x bonds and the other layer with short y bonds and (2) one layer with short x_1 and y_2 bonds and the other layer with short x_2 and y_1 bonds are also considered and plotted, denoted as xx-yy and xy-yx, respectively. It turns out these bilayer structures are not energetically favored.

Figure 2(c) shows the changes of bond ordering during phase transitions by plotting bond lengths versus pressure. The bond lengths change dramatically between 35 and 45 GPa, corresponding to two structural phase transitions discussed above. The bond ordering can be summarized as $l_x = l_y \lesssim l_z$ for $C2/m$-zigzag, $l_x < l_y \approx l_z$ for $P\bar{1}$ and $l_{x_1} = l_{y_2} < l_{x_2} = l_{y_1} \approx l_z$ for $P2_1/m$, which is consistent with the above discussions for Figs. 1(c)–1(e).

Previous finding suggests that the magnetic configuration is sensitive to structure deviations [13]. We then examine the magnetic structure of the $C2/m$-zigzag structure during the structural phase transition under pressure. Figure 2(d) shows the total magnetic moment magnitude and its angle to the $\boldsymbol{a}$ axis of the $C2/m$-zigzag structure under various pressures, where the moment direction rotates in the ac plane roughly
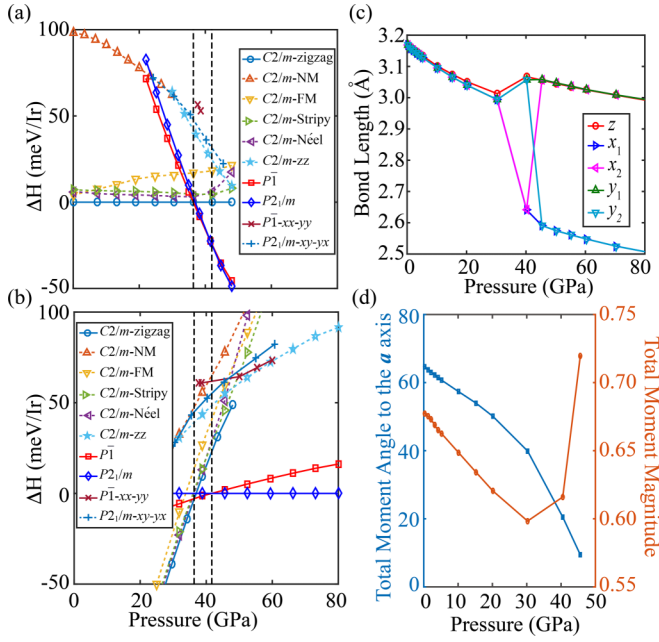
FIG. 2. Calculated static lattice enthalpy of different structures relative to (a) the $C2/m$-zigzag structure and (b) the $P2_1/m$ structure, respectively. (c) Calculated bond lengths vs pressure, which reflects the changes of bond ordering. (d) Calculated total moment magnitude and angle to the a axis of the $C2/m$-zigzag structure under various pressures.

from $a + c$ to a as pressure increases. The moment rotation is likely to be a consequence of the slight increase of the ratio l_z/l_x as pressure increases, where the ratio trend is clearly shown in Fig. 2(c). As for the magnitude of the magnetic moment, first it decreases gradually until about 30 GPa, and then goes up abruptly after 40 GPa, indicating a magnetic transition at around 30–40 GPa, which is consistent with our previous discussions.

It should be remarked that $P\bar{1}$ and $P2_1/m$ do not appear to be even metastable for $P < 22$ GPa. $C2/m$-zigzag cannot exist for pressures higher than about 48 GPa [Figs. 2(a) and 2(b)]: (1) For $48 < P \leqslant 56$ GPa, an imaginary phonon frequency appears at Γ (only Γ is calculated for cost reasons), indicating the structure instability; (2) for $P > 56$ GPa, $C2/m$-zigzag relaxes automatically to $P\bar{1}$ or $P2_1/m$. Situations are similar for other $C2/m$ magnetic structures, i.e., they disappear above certain pressures [Figs. 2(a) and 2(b)]: (1) An imaginary phonon frequency appears at Γ between 40 and 50 GPa for FM, Néel, and NM, and between 50 and 60 GPa for stripy; (2) they relax automatically to $P\bar{1}$ or $P2_1/m$ above a pressure between 60 and 70 GPa for FM and stripy, between 50 and 60 GPa for Néel, and between 70 and 80 GPa for NM.

The results presented so far, based on the static lattice approximation, already indicate the appearance of a rich phase diagram for Na$_2$IrO$_3$ under pressure. We further take into account the effects of lattice vibrations by including the phonon free energy still within the Born-Oppenheimer approximation. We calculate the phonon dispersions of $C2/m$-zigzag, $P\bar{1}$, and $P2_1/m$ under different pressures to obtain the zero-point energy corrections (phonon free energy at zero temperature).
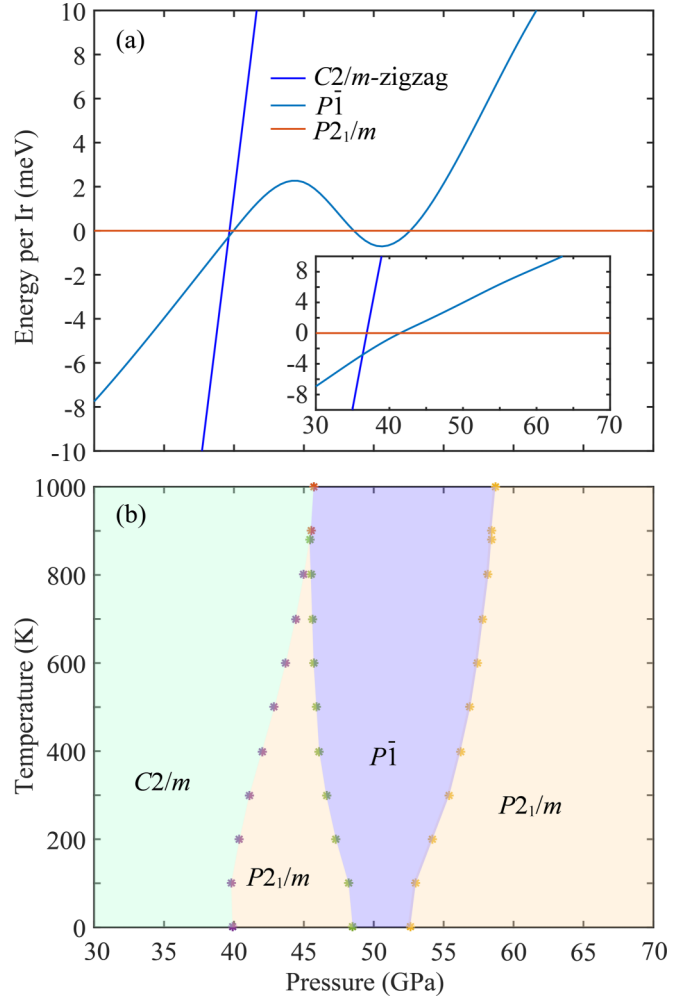

FIG. 3. (a) The static lattice enthalpy of $C2/m$-zigzag, $P\bar{1}$, and $P2_1/m$ structures with zero-point energy corrections. The inset in (a) shows the results without zero-point energy corrections for comparison. (b) The pressure vs temperature phase diagram considering the phonon free energy.

The results are shown in Fig. 3(a). The inset in Fig. 3(a) shows the results without zero-point energy corrections for comparison. It can be seen that under pressures lower than 40 GPa, $C2/m$-zigzag is still the most stable structure. For pressures higher than 53 GPa, $P2_1/m$ is the most stable. However, the stability range of pressure for $P\bar{1}$ shrinks to a point in contrast to $\sim$5 GPa without zero-point energy corrections. In other words, with the increase of pressure, Na$_2$IrO$_3$ will first undergo a phase transition from $C2/m$-zigzag magnetic order to $P2_1/m$ NM order. We also find that $P\bar{1}$ reenters as the most stable structure between 48 and 53 GPa. In Fig. 3(b), we plot the calculated phase diagram considering the phonon free energy. It is worth mentioning that in a relatively large temperature range, Na$_2$IrO$_3$ will undergo successive phase transitions, $C2/m \rightarrow P2_1/m \rightarrow P\bar{1} \rightarrow P2_1/m$, with the increase of pressure.

In order to clarify the phonon modes responsible for the zero-point vibration-driven stabilization of the $P\bar{1}$ phase, we calculate the phonon density of states and the differences of integrated zero-point vibration energies of the $P\bar{1}$
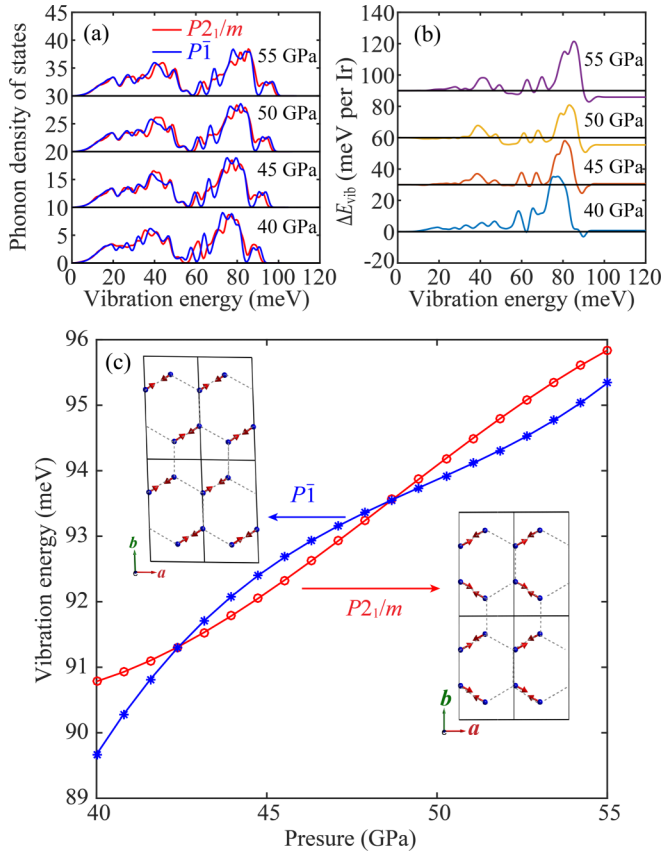
FIG. 4. (a) Calculated phonon density of states of the $P\bar{1}$ and $P2_1/m$ structures under different pressures. (b) The differences of integrated zero-point vibration energies of the $P\bar{1}$ and $P2_1/m$ structures under different pressures. (c) The evolution of the vibration energies of the dimerization modes with pressure. The insets in (c) are the dimerization modes of the $P\bar{1}$ and $P2_1/m$ structures, where only the vibrations of Ir atoms are shown. The gray dashed lines in the insets are guides to the eye for the Ir honeycomb lattice.

and $P2_1/m$ structures under different pressures across the phase transitions, and the results are shown in Figs. 4(a) and 4(b). The integrated zero-point vibration energies $E_{\mathrm{vib}}(\omega)$ are defined by

$$E_{\mathrm{vib}}(\omega) = \frac{1}{2}\hbar \int_0^\omega \rho_{\mathrm{ph}}(\omega')\omega' d\omega',$$

where ρ_{ph} is the phonon density of states. The difference of integrated zero-point vibration energies is given by $\Delta E_{\mathrm{vib}}(\omega) = E_{\mathrm{vib}}(\omega)|_{P\bar{1}} - E_{\mathrm{vib}}(\omega)|_{P2_1/m}$. It can be clearly seen that the contributions from the acoustic modes of the $P\bar{1}$ and $P2_1/m$ structures (with vibration energies below 25 meV, as shown in Fig. S2 in the Supplemental Material [35]) are nearly the same for all the pressures. The differences are mainly from the optical modes with energy between 50 and 100 meV, especially around 85 meV, as displayed in Fig. 4(b). This can be well understood from the phonon dispersion as shown in Fig. S2 in the Supplemental Material [35]. There is a gap around 85 meV in the phonon dispersion of the $P\bar{1}$ structure, which will drive the modes $\lesssim 85$ meV softer compared to that of the $P2_1/m$ structure.

Since the $P\bar{1}$ and $P2_1/m$ structures do not share the same normal vibration modes, it is difficult to compare their vibration modes directly. However, the dimerization modes (with $\mathbf{q} = 0$) of the $P\bar{1}$ and $P2_1/m$ structures (with vibration energies around 90 meV) are representative modes that are responsible for the phonon-driven stabilization of the $P\bar{1}$ phase, as indicated in Fig. 4(b). The evolution of the vibration energies of the dimerization modes with pressure are shown in Fig. 4(c). The vibration energies of these dimerization modes all increase with the increase of pressure. The evolution trend of the vibration energy of the dimerization modes with pressure roughly gives the phase transition pressures of the $P\bar{1}$ and $P2_1/m$ structures. However, since there are many phonon modes contributing to the stabilization of the $P\bar{1}$ phase, the transition pressures are not determined directly by the dimerization modes, as is identified here. In the pressure above about 50 GPa, it is worth mentioning that the $P\bar{1}$ structure has a lower phonon energy with respect to the $P2_1/m$ structure [see Fig. 4(b)], and that the $P2_1/m$ structure has a lower electronic energy with respect to the $P\bar{1}$ structure [see the inset in Fig. 3(a)]. When its disadvantage from electronic energy is compensated by the advantage from lattice vibration, the $P\bar{1}$ structure becomes the most stable phase around 50 GPa. This scenario of phase transition from a competition between electronic and vibrational energy may be helpful to understand the bond-order-dependent energy variation in Na_2IrO_3 and similar systems having a honeycomb lattice structure.

In order to investigate the $J_{\mathrm{eff}} = 1/2$ feature of Na_2IrO_3 during phase transitions, we construct a first-principles-based Wannier tight-binding model [36]. There are four Ir atoms in each unit cell. Each Ir^{4+} ion has five $5d$ electrons, occupying six t_{2g} orbitals due to crystal-field splitting, assuming the Ir-O octahedra remain regular during the crystal phase transitions. As a result of strong SOC, the six t_{2g} orbitals are further separated into two manifolds with $J_{\mathrm{eff}} = 3/2$ and $J_{\mathrm{eff}} = 1/2$. We then decompose the band structures into $J_{\mathrm{eff}} = 3/2$ and $J_{\mathrm{eff}} = 1/2$ components. The results are plotted in the fat bands in Figs. 5(a)–5(c), where the linewidth represents the weight of the $J_{\mathrm{eff}} = 1/2$ states. We also calculate the averaged weight of $J_{\mathrm{eff}} = 1/2$. For a band, it is defined by $\sum_{\mathbf{k}} W_{1/2}(\mathbf{k}) / \sum_{\mathbf{k}} W_{t_{2g}}(\mathbf{k})$, where $W_{1/2}(\mathbf{k})$ and $W_{t_{2g}}(\mathbf{k})$ are the spectral weights of $J_{\mathrm{eff}} = 1/2$ and the t_{2g} orbitals, respectively. Since the first-principles-based Wannier tight-binding models are constructed by the t_{2g} orbitals of Ir atoms, $\sum_{\mathbf{k}} W_{t_{2g}}(\mathbf{k})$ is just $N_{\mathbf{k}}$. For the eight bands around the Fermi level, the averaged weight of $J_{\mathrm{eff}} = 1/2$ is 0.784, 0.681, and 0.662 for $C2/m$-zigzag, $P\bar{1}$, and $P2_1/m$ in Fig. 5, respectively. The weight of $J_{\mathrm{eff}} = 1/2$ for $P\bar{1}$ and $P2_1/m$ shows a reduction compared with that for $C2/m$-zigzag, which can be considered as a consequence of the change of bond ordering. In $P\bar{1}$ and $P2_1/m$, the appearance of shorter Ir-Ir bonds will lead to larger nearest-neighbor hopping, which in turn results in a larger band splitting. Indeed, Fig. 5 clearly shows that the overall band splitting in $C2/m$-zigzag is the smallest and that in $P2_1/m$ the largest, which is consistent with the calculated average weight of $J_{\mathrm{eff}} = 1/2$. Although the weights differ in these structures, $J_{\mathrm{eff}} = 1/2$ states are still the main components around the
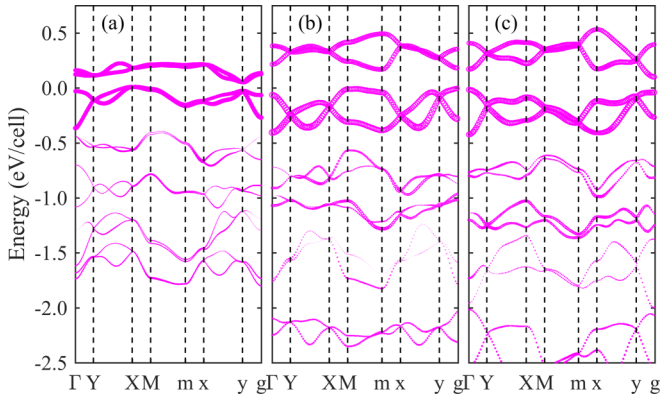
FIG. 5. Calculated tight-binding band structures (four Ir per unit cell) with SOC of (a) $C2/m$-zigzag, (b) $P\bar{1}$, and (c) $P2_1/m$, at 48 GPa, respectively. Fat bands are plotted for band structures with SOC (without Hubbard U), where the linewidth represents the weight of the $J_{\text{eff}} = 1/2$ states. The high-symmetry **k** points are $\Gamma(0, 0, 0)$, $Y(0, 1/2, 0)$, $X(1/2, 0, 0)$, $M(1/2, 1/2, 0)$, $m(1/2, 1/2, 1/2)$, $x(1/2, 0, 1/2)$, $y(0, 1/2, 1/2)$, and $g(0, 0, 1/2)$.

Fermi level. Also, the $J_{\text{eff}} = 3/2$ states are fully filled and $J_{\text{eff}} = 1/2$ states are half filled, which are consistent with our expectations.

In summary, we study the bond-ordering-induced phase transitions in Na$_2$IrO$_3$ under high pressure by first-principles calculations. We find that the Na$_2$IrO$_3$ crystal will undergo successive structural and magnetic phase transitions, $C2/m \rightarrow P2_1/m \rightarrow P\bar{1} \rightarrow P2_1/m$, with the increase of pressure, where the $C2/m$ structure holds a zigzag magnetic order, while $P2_1/m$ and $P\bar{1}$ are both nonmagnetic. $C2/m$ is classified as a Mott insulator, while $P2_1/m$ and $P\bar{1}$ are

all band insulators. The low-energy excitations of these bond-ordered high-pressure phases can be well described by the $J_{\text{eff}} = 1/2$ states. Considering that the $P\bar{1}$ phase possesses a $l_x < l_y \approx l_z$ bond ordering as well as its $J_{\text{eff}} = 1/2$ nature, we may expect that it bears a remarkable resemblance to the gapped A phase of the Kitaev ground state [1]. However, a recent experiment on RuCl$_3$, which shows a similar bond-ordered phase with respect to that in Na$_2$IrO$_3$ under pressure, suggests the suppression of the Kitaev interaction-driven magnetic ground state [27]. As the DFT mean field yields a nonmagnetic phase, we cannot devise a sensible model to determine if the interaction parameters are lying in the Kitaev A-phase region in this work. The uncertainty calls for further theoretical and experimental investigations. Band structures and phonon dispersions are calculated for comparison to future experiments. Together with previous high-pressure experiments on α-Li$_2$IrO$_3$ [17] and α-RuCl$_3$ [25–27], we may infer that structural and magnetic transitions driven by external pressure are universal in these Kitaev candidate materials. The bond-ordered phases found in our work may also exist in other candidates in a certain range of pressure, which will enrich the phase diagrams of these materials.

[1] A. Kitaev, Ann. Phys. **321**, 2 (2006).

[2] G. Jackeli and G. Khaliullin, Phys. Rev. Lett. **102**, 017205 (2009).

[3] J. Chaloupka, G. Jackeli, and G. Khaliullin, Phys. Rev. Lett. **105**, 027204 (2010).

[4] Y. Singh and P. Gegenwart, Phys. Rev. B **82**, 064412 (2010).

[5] X. Liu, T. Berlijn, W.-G. Yin, W. Ku, A. Tsvelik, Y.-J. Kim, H. Gretarsson, Y. Singh, P. Gegenwart, and J. P. Hill, Phys. Rev. B **83**, 220403(R) (2011).

[6] S. K. Choi, R. Coldea, A. N. Kolmogorov, T. Lancaster, I. I. Mazin, S. J. Blundell, P. G. Radaelli, Y. Singh, P. Gegenwart, K. R. Choi, S.-W. Cheong, P. J. Baker, C. Stock, and J. Taylor, Phys. Rev. Lett. **108**, 127204 (2012).

[7] F. Ye, S. Chi, H. Cao, B. C. Chakoumakos, J. A. Fernandez-Baca, R. Custelcean, T. F. Qi, O. B. Korneta, and G. Cao, Phys. Rev. B **85**, 180403(R) (2012).

[8] S. W. Lovesey and A. N. Dobrynin, J. Phys.: Condens. Matter **24**, 382201 (2012).

[9] S. H. Chun, J.-W. Kim, J. Kim, H. Zheng, C. C. Stoumpos, C. D. Malliakas, J. F. Mitchell, K. Mehlawat, Y. Singh, Y. Choi, T. Gog, A. Al-Zein, M. Moretti Sala, M. Krisch, J. Chaloupka,

G. Jackli, G. Khalliullin, and B. J. Kim, Nat. Phys. **11**, 462 (2015).

[10] K. A. Modic, T. E. Smidt, I. Kimchi, N. P. Breznay, A. Biffin, S. Choi, R. D. Johnson, R. Coldea, P. Watkins-Curry, G. T. McCandless, J. Y. Chan, F. Gandara, Z. Islam, A. Vishwanath, A. Shekhter, R. D. McDonald, and J. G. Analytis, Nat. Commun. **5**, 4203 (2014).

[11] T. Takayama, A. Kato, R. Dinnebier, J. Nuss, H. Kono, L. S. I. Veiga, G. Fabbris, D. Haskel, and H. Takagi, Phys. Rev. Lett. **114**, 077202 (2015).

[12] S. C. Williams, R. D. Johnson, F. Freund, S. Choi, A. Jesche, I. Kimchi, S. Manni, A. Bombardi, P. Manuel, P. Gegenwart, and R. Coldea, Phys. Rev. B **93**, 195158 (2016).

[13] K. Hu, F. Wang, and J. Feng, Phys. Rev. Lett. **115**, 167204 (2015).

[14] J. G. Rau, E. K.-H. Lee, and H.-Y. Kee, Phys. Rev. Lett. **112**, 077204 (2014).

[15] Y. Yamaji, Y. Nomura, M. Kurita, R. Arita, and M. Imada, Phys. Rev. Lett. **113**, 107201 (2014).

[16] V. M. Katukuri, S. Nishimoto, V. Yushankhai, A. Stoyanova, H. Kandpal, S. Choi, R. Coldea, I. Rousochatzakis,

L. Hozoi, and J. van den Brink, New J. Phys. **16**, 013056 (2014).

[17] V. Hermann, M. Altmeyer, J. Ebad-Allah, F. Freund, A. Jesche, A. A. Tsirlin, M. Hanfland, P. Gegenwart, I. I. Mazin, D. I. Khomskii, R. Valenti, and C. A. Kuntscher, Phys. Rev. B **97**, 020104(R) (2018).

[18] V. Hermann, J. Ebad-Allah, F. Freund, I. M. Pietsch, A. Jesche, A. A. Tsirlin, J. Deisenhofer, M. Hanfland, P. Gegenwart, and C. A. Kuntscher, Phys. Rev. B **96**, 195137 (2017).

[19] X. Zhou, H. Li, J. A. Waugh, S. Parham, H.-S. Kim, J. A. Sears, A. Gomes, H.-Y. Kee, Y.-J. Kim, and D. S. Dessau, Phys. Rev. B **94**, 161106(R) (2016).

[20] X.-L. Sheng and B. K. Nikolić, Phys. Rev. B **95**, 201402(R) (2017).

[21] M. Abramchuk, C. Ozsoy-Keskinbora, J. W. Krizan, K. R. Metz, D. C. Bell, and F. Tafti, J. Am. Chem. Soc. **139**, 15371 (2017).

[22] K. Kitagawa, T. Takayama, Y. Matsumoto, A. Kato, R. Takano, Y. Kishimoto, S. Bette, R. Dinnebier, G. Jackeli, and H. Takagi, Nature (London) **554**, 341 (2018).

[23] S.-H. Baek, S.-H. Do, K.-Y. Choi, Y. S. Kwon, A. U. B. Wolter, S. Nishimoto, J. van den Brink, and B. Büchner, Phys. Rev. Lett. **119**, 037201 (2017).

[24] J. Zheng, K. Ran, T. Li, J. Wang, P. Wang, B. Liu, Z.-X. Liu, B. Normand, J. Wen, and W. Yu, Phys. Rev. Lett. **119**, 227208 (2017).

[25] Y. Cui, J. Zheng, K. Ran, J. Wen, Z.-X. Liu, B. Liu, W. Guo, and W. Yu, Phys. Rev. B **96**, 205147 (2017).

[26] Z. Wang, J. Guo, F. F. Tafti, A. Hegg, S. Sen, V. A. Sidorov, L. Wang, S. Cai, W. Yi, Y. Zhou, H. Wang, S. Zhang, K. Yang, A. Li, X. Li, Y. Li, J. Liu, Y. Shi, W. Ku, Q. Wu, R. J. Cava, and L. Sun, Phys. Rev. B **97**, 245149 (2018).

[27] G. Bastien, G. Garbarino, R. Yadav, F. J. Martinez-Casado, R. Beltrán Rodríguez, Q. Stahl, M. Kusch, S. P. Limandri, R. Ray, P. Lampen-Kelley, D. G. Mandrus, S. E. Nagler, M. Roslova, A. Isaeva, T. Doert, L. Hozoi, A. U. B. Wolter, B. Büchner, J. Geck, and J. van den Brink, Phys. Rev. B **97**, 241108(R) (2018).

[28] G. Kresse and J. Hafner, Phys. Rev. B **47**, 558(R) (1993).

[29] G. Kresse and J. Furthmüller, Phys. Rev. B **54**, 11169 (1996).

[30] G. Kresse and D. Joubert, Phys. Rev. B **59**, 1758 (1999).

[31] D. van der Marel and G. A. Sawatzky, Phys. Rev. B **37**, 10674 (1988).

[32] S. L. Dudarev, G. A. Botton, S. Y. Savrasov, C. J. Humphreys, and A. P. Sutton, Phys. Rev. B **57**, 1505 (1998).

[33] K. Parlinski, Z. Q. Li, and Y. Kawazoe, Phys. Rev. Lett. **78**, 4063 (1997).

[34] A. Togo and I. Tanaka, Scr. Mater. **108**, 1 (2015).

[35] See Supplemental Material at http://link.aps.org/supplemental /10.1103/PhysRevB.98.100103 for discussions on (1) the stability of Na_2IrO_3 under pressure, (2) structure stabilities of the $C2/m$-zigzag, $P\bar{1}$, and $P2_1/m$ phases, and (3) band structures of the $C2/m$-zigzag, $P\bar{1}$ and $P2_1/m$ phases.

[36] A. A. Mostofi, J. R. Yates, G. Pizzi, Y.-S. Lee, I. Souza, D. Vanderbilt, and N. Marzari, Comput. Phys. Commun. **185**, 2309 (2014).